Guided-Wave Planar Optical Interconnects Using Highly Multiplexed Polymer Waveguide Holograms

Ray T. Chen, Huey Lu, Daniel Robinson, Michael Wang, Gajendra Savant, and Tomasz Jannson

Abstract— **A new intraplanar interconnection scheme using substrate guided modes in conjunction with a highly multiplexed waveguide volume hologram is presented. 1-to-50 passive and 1-to-2-to-100 acoustooptically addressed reconfigurable interconnections were demonstrated with a fan-out diffraction efficiency of 55% at 514-nm wavelength. A coordinate transformation converts the three-dimensional (3-D) diffraction problem into a two-dimensional (2-D) one which significantly simplifies the theoretical calculation. Intraplane massive fan-out optical interconnection using substrate guided mode provides us with both collinear and coplanar fan-out capability for data and clock signals. Collinearity of signal distribution allows us to process the 2-D input signal array which is not achievable using conventional single-mode integrated optical devices. The applicability of the reported concept can be transferred to any substrate of interest, such as GaAs and Si, as long as the transparency of the substrate holds. The laminated waveguide device containing a highly multiplexed dichromated gelatin (DCG) hologram was evaluated. It demonstrated an outstanding survivability in harsh environments, including low and high temperature (−100 to +180°C), water immersion, laser damage threshold (10 kJ/cm^2), and nuclear radiation hardening (under 63-Mev proton >2 Mrad (Si), and ^{60}Co Gamma Ray >2 Mrad (Si) without loss of diffraction efficiency). Finally, we present the most attractive applications, including intrawafer clock signal distribution, backplane optical interconnection, surface enhanced Raman scattering (SERS) sensor, head-up displays, and module-to-module optical interconnection.**

I. Introduction

THE proliferation of radio frequency (RF) and microwave signal communications has highlighted the severe limitations of current interconnect capabilities. These communications, which are implemented in either analog or digital formats, require interconnects with time and space multiplexibility, i.e., high-speed performance, high fan-out and reasonable distances. As the number of components per chip, the modulation speed and the degree of integration continues to increase, electrical interconnection will soon become inadequate on the intra-module and module-to-module level. For example, with a clock speed of 1 Gb/s, electrical interconnects can only provide us with a mm to cm communication distance [1], which seriously limits the scale of integration. Various interconnection hierarchies are summarized in Table I. Currently, VLSI ON-chip interconnection has two to five vertical levels of integration. The major concern is to provide high-speed interconnection from chip to chip, module to module, board to board, and machine to machine. Optical interconnects have particularly been of interest at levels where the speed and communication distance are beyond the capability of electrical interconnects. Moreover, it is also true that approximately 90% of electronic failures are attributable to packaging and board interconnection. Evolution of electronic packaging and interconnection from a single chip device to a surface mount device (SMD) to a multichip module (MCM) has mainly concentrated on improving the system performance speed and the reliability. The concept we presented in this paper is useful for all interconnection scenarios except for machine-to-machine interconnection where an optical fiber is the element of choice. MCM technologies push system performance to higher clock speeds with increased circuit densities and, thus, shorten the chip-to-chip interconnection distance. The need for imposing an optical interconnection network on optoelectronic systems is obvious given that state-of-the-art electrical interconnection and packaging can not provide us with required clock speeds and communication distances.

At the board level, the limitations of pins on the electrical interconnect capability has become a critical issue. Rents Rule says that the number of interconnections U is equal to $U^{2/3}$, where U is the number of devices [2]. However, the minimum spacing between interconnections required by this rule happens to be ~5 times smaller than the minimum allowed pin spacing needed to avoid signal cross coupling in typical chips. This problem is solved by using an optical interconnect in which the minimum space between the interconnects is the size of a single-mode waveguide. Furthermore, on chip high power sources are required to drive electrical interconnects, which is not the case for optical interconnects. Finally, unacceptable coupling between lines occurs at high speed with electrical interconnects while no coupling results with optical interconnects. Because of all of these considerations, optical interconnects are well suited to VLSI chip-to-chip, intrawafer-scale integrated circuits and three-dimensional board-to-board communications where the problems resulting from the use of electrical interconnections are serious. This is because increasing fan-out reduces the effective impedance along the electrical interconnects and increases its propagation delay [3], thereby reducing its communication distance. The density of optical interconnects may be high since cross talk is not affected by the signal bandwidth and optical channels may cross in space without interaction.

In this paper, both experimental results and further applications of optical interconnection architectures based on

Manuscript received March 1, 1991; revised February 9, 1992. This research project was sponsored by DARPA, Wright Patterson AFB and Army Harry Diamond Lab.

The authors are with Physical Optics Corporation, Torrance, CA 90505.

IEEE Log Number 9108296.

TABLE I
INTERCONNECTION HIERARCHY

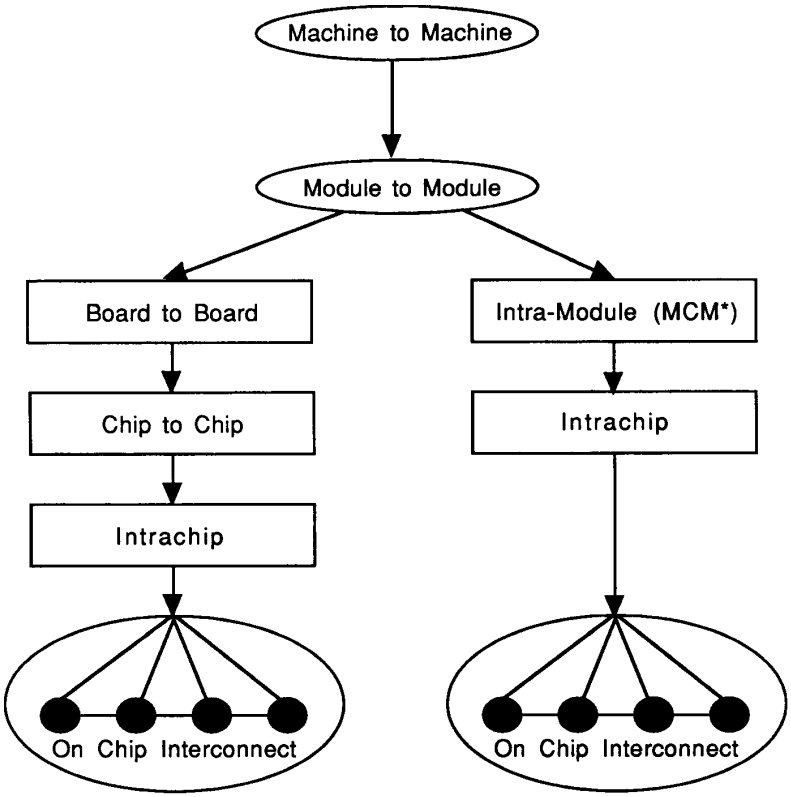

* Multichip Module

the fundamental building blocks, including holographic and guided wave optical elements, are presented. Note that the substrate guided mode [4] defined herein was usually defined as substrate mode in integrated optics. In Section II, formulas derived from the coupled wave theory [4], [5] are introduced. Diffraction efficiency, as a function of the intra-plane diffraction angle, the grating index modulation, the interaction length and the dephasing factor, is further described. The angular selectivity and fan-out density are also discussed. In Section III, the recording and reconstruction setup for a waveguide massive fan-out hologram is presented. Experimental results on 1-to-N and 1-to-2-to $2N$ guided wave fan-outs are demonstrated with $N = 50$ at wavelength of 514.5 nm in Section IV. In Section V, the reliability test of the intraplane guided wave fan-out device is also evaluated. Survivability of the laminated DCG waveguide device in harsh environments, including temperature fluctuation from $-100°C$ to $+180°C$, laser damage test under 10 kJ/cm^2 and water boiling test, is experimentally confirmed. Finally, an array of applications, including backplane and intrawafer optical interconnections, a surface-enhanced Raman sensor and a head up display, are further described in Section VI.

II. COUPLED WAVE THEORY

Planar amplitude and phase holograms are of wide interest because of their many applications to optical interconnects, guided wave optics, and spectroscopy. The two most common methods of analyzing intraplane holographic diffraction are the coupled-wave approach [6]–[13] and the model approach [14]–[24]. Our investigations were restricted to the case of a grating vector **K** lying in the plane of incidence (the plane is defined by the wave normal and the boundary normal). In this situation, the TE (transverse electric, i.e., electric field perpendicular to the plane of incidence) and the TM (transverse magnetic, i.e,g, magnetic field perpendicular to the plane of incidence) components of the input plane wave are completely decoupled and may be treated separated. However, in the general case, the grating vector may have any arbitrary orientation with respect to the plane of incidence. In this situation, the TE and TM components of the input plane wave are coupled inside the grating and may not be treated separately. For a thick transmission hologram, only one diffraction at or near the Bragg angle will be possible. The present work, using the coupled wave approach, gives the solution for thick transmission phase grating for the general

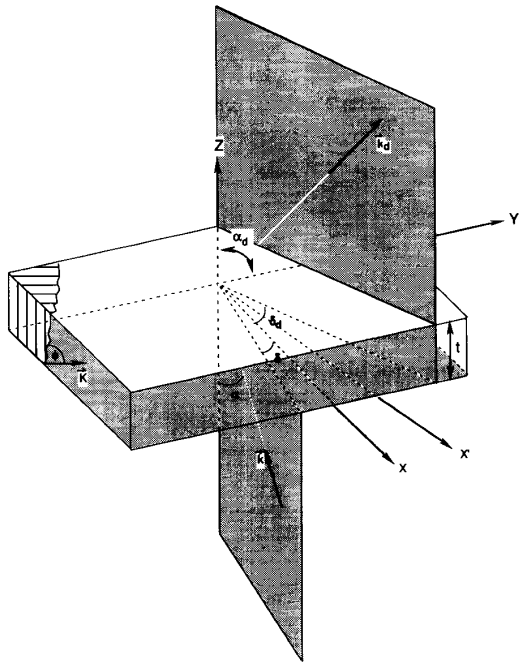

Fig. 1. Model of a three-dimensional diffraction by a slanted planar phase hologram.

3-D diffraction geometry.

The general 3-D grating diffraction problem is depicted in Fig. 1. A linearly polarized electromagnetic wave is obliquely incident at an arbitrary angle α on a slanted-fringe phase planar grating of slant angle Φ bounded by two different homogeneous media. The planar grating has an arbitrary direction. It may be characterized by a periodic index modulation as

$$n \cong n_o + \Delta n \cos\left(\vec{K} \cdot \vec{r}\right) \tag{1}$$

where n_o is the index of refraction of the unperturbed region and Δn is the amplitude of the associated index modulation. A simplified method of solving the 3-D diffraction problem, without degrading the data required, is to generate a new coordinate system such that the incident, diffracted and grating wave vectors located in the same coordinate plane. With such an arrangement, the incident and diffracted wave can be decomposed into $\|$ (parallel) and $\perp$ (perpendicular) polarizations. There is no cross-coupling between $\|$ and $\perp$ polarized light after coordinate transformation. As a consequence, the incident beam with arbitrary polarization, e.g., TE, TM or the combination of TE and TM, can be decomposed into $\|$ and $\perp$ components [25]. Such an arrangement converts the 3-D problem into a two-dimensional (2-D) problem, which significantly simplifies the complexity of the mathematics [4], [25].

The resultant diffraction efficiency is simply the linear combination of $\|$ and $\perp$ components of the diffracted light. Note that when the electric field of an optical wave is parallel to the diffraction plane, it is defined as $\|$ polarization. $\perp$ polarization occurs when the optical wave has its electric field perpendicular to the diffraction plane. The resultant diffracted beams are the vector summation of the diffracted $\|$ and $\perp$ polarized beams. Fig. 2(a) shows an $x - y - z$ coordinate system. The z axis is perpendicular to the grating vector $\mathbf{K}$. The $x - z$ plane is overlapped with the triangle constructed by $\mathbf{k}_d$ (diffracted) $\mathbf{k}$ (incident), and the grating vector $\mathbf{K}$. for the transmission hologram shown in Fig. 2(b), the diffraction efficiencies $\eta_{\|}$ and $\eta_{\perp}$ for each individual hologram are given by [25]

$$\eta_{\perp} = \frac{4\kappa^2}{(C_r/C_\delta)\vartheta^2 + 4\kappa^2} \sin^2\left[\frac{1}{2}\left(\frac{\vartheta^2}{C_\delta^2} + \frac{4\kappa^2}{C_r C_\delta}\right)^{1/2} d\right] \tag{2}$$

and

$$\eta_{\|} = \frac{4\kappa^2\left(\hat{k}\cdot\hat{k}_d\right)^2}{\left(C_r/C_\delta\right)\vartheta^2 + 4\kappa^2\left(\hat{k}\cdot\hat{k}_d\right)^2} \times \sin^2\left[\frac{1}{2}\left(\frac{\vartheta^2}{C_\delta^2} + \frac{4\kappa^2\left(\hat{k}\cdot\hat{k}_d\right)^2}{C_r C_\delta}\right)^{1/2} d\right] \tag{3}$$

where

$$C_r = k_z/k_o, \quad C_\delta = k_{dz}/k_o, \quad \kappa = \pi\Delta n/\lambda$$

d is the grating interaction length, k_z and k_{dz} are the $\hat{z}$ components of $\mathbf{k}$ and $\mathbf{k}_d$, $k_o = 2\pi n/\lambda$, ϑ is the dephasing factor, $\hat{k}$ and $\hat{k}_d$ are the unit vectors for the incident and diffracted wave propagation constants. As indicated in Fig. 2(a), the diffraction plane is defined by the plane of the triangle constructed with $\mathbf{K}$, $\mathbf{k}$, and $\mathbf{k}_d$. $\eta_{\|}$ and $\eta_{\perp}$ are the diffraction efficiencies of the substrate guided waves with polarizations parallel and perpendicular, respectively, to the diffraction plane. For the case of Bragg condition, which implies the perfect phase matching, we have

$$\eta = a\eta_{\|} + (1-a)\eta_{\perp} \tag{4}$$

for an arbitrarily polarized light. In (4), a and (1a) represent the percentage of the intensity of the incident light corresponding to $\|$ and $\perp$ polarization, respectively. Note that the maximum diffraction efficiency for $\eta_{\|}$ and $\eta_{\perp}$ do not occur simultaneously under the same device parameters associated in (2) and (3). The out-of-phase behavior (with respect to the grating thickness d) causes the total normalized diffracted field to be less than unity. The diffraction efficiency does not reach 100% unless an incident wave with purely $\|$ or $\perp$ polarization, in conjunction with the optimized Δn and d values, can be arranged. In the case of a conventional single-mode integrated optics device, TE and TM modes are well described by the $\|$ and $\perp$ polarization defined herein. As a result, the formulas derived in this paper are also applicable to the single-mode case [26]. A detailed presentation of the 2-D diffraction theory can be found in [25].

Optical interconnections with massive fan-outs require high efficiency and low crosstalk. High efficiency can be achieved by carefully controlling the incident angles and polarizations as

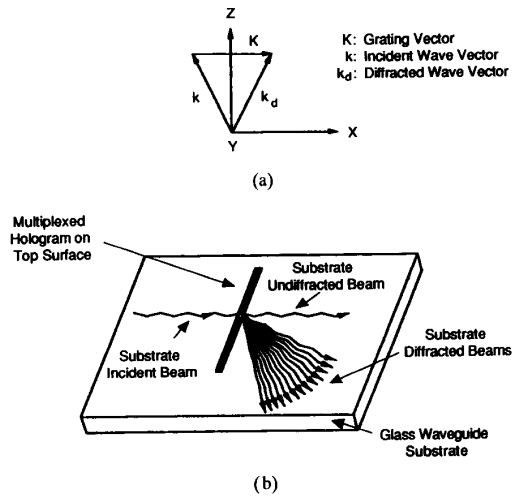

Fig. 2. (a) Definition of an $x-y-z$ coordinate, and (b) a schematic of an intraplane one-to many fan-out using a transmission hologram.

well as the grating parameters. The low crosstalk for massive fan-outs requires minimal angular overlap between adjacent fan-out channels. Thus, the angular selectivity of the Bragg hologram is the key to determining the theoretical massive fan-out capability. For a given grating modulation index, a decrease in angular bandwidth can be achieved but it requires either an increase in the grating interaction length or an increase in the Bragg angle. Furthermore, the diffracted beam size Ω is represented by

$$\Omega = 2d\tan\delta + wcsc\delta \tag{5}$$

where d is the interaction length, w is the aperture of the incident laser beam, and δ is the Bragg diffraction angle. To integrate the planar waveguide device with mutli-mode fibers, such as 50/125, 62.5/125, and 100/140 μm in size, the value of Ω (d, w, δ) needs to be reduced to the core size of the associated fiber. It is clear that there is a tradeoff between the interaction length and the diffraction efficiency, while maintaining a good mode match between the multimode waveguide output and the output fiber. Our experimental results indicate that the mode profile of the substrate multi-mode guided wave also demonstrated an azimuthal symmetry [27], which is equivalent to the fiber-guided mode. Excellent coupling efficiency from the waveguide to the fiber, and vice versa, is expected.

Unlike electrical interconnects, the massive fan-out optical means does not involve excess capacitance. The number of fan-outs is primarily limited by two factors: (1) angular selectivity of the adjacent channel, which determines the closeness of the 1-to-many fan-out, and (2) power budget of the interconnect which is correlated with the speed of the data and clock signals and the sensitivity of the receiver. The maximum fan-out available, without jeopardizing the demodulation process, is given by [28]

$$N = \frac{(1-\xi)\cdot I_{op}}{P_{\min}} \tag{6}$$

where I_{op} is the optical input intensity and ξ is the insertion loss from the transmitter to the receiver. For an analog signal [28]

$$P_{\min} \approx 2\sqrt{\pi}\,\frac{h\nu\cdot f}{e\xi}\,\sqrt{kT_nC_d} \tag{7}$$

for a p-i-n/FET receiver, and

$$P_{\min} \approx 2\,\frac{h\nu\cdot f}{Me\xi}\,\frac{\sqrt{kT_nf}}{R} \tag{8}$$

for an avalanche photodiode. In (7) and (8), hν is the photon energy, f is the modulation bandwidth, e is the charge of an electron, T_n is the effective noise temperature, R_L is the loading resistance, C_d is the capacitance of the photodetector, ζ is the quantum efficiency, and M is the photocurrent multiplication. Equations (7) and (8) were derived by assuming that the minimum detectable power is the power input for which S/N, i.e., signal/noise ratio, equals 1. For a digital optical interconnection system, the required modulation speed (b/s) and the bit error rate specify the RC constant of the detector and the S/N ratio, respectively. The minimum detectable power can be easily decided. For example, a digital transmission system with 5×10^9 b/s and an error probability at the receiver less than 5×10^{-10}, based on the error probability function, has a [28] $S/N = 12.9$ (i.e., 22.2 dB) and RC $= \frac{1}{2\pi\Delta\nu} = \frac{\tau}{4} = 5\times10^{-11}$. With known effective noise temperature and quantum efficiency, (7) and (8) can be easily modified to provide the numerical value of the $P_{\min}$.

III. Recording of a Waveguide Fan-Out Hologram

To construct the holographic gratings, the recording setup shown in Fig. 3 is used (other geometries are possible). Depending upon the absorption characteristics of the holographic emulsion, proper recording beams need to be chosen. Various types of transmission holograms can be constructed by using this setup. The grating space Λ is given by

$$\Lambda = \frac{\lambda}{2n\sin\theta} \tag{9}$$

in an unslanted grating. In (9), λ is the recording wavelength, θ is the half angle of two incident beams and n is the refractive index of the medium on top of the holographic emulsion ($n = 1$ for air). For an intraplane optical interconnection, the grating vector K, which is defined as $2\pi/\Lambda$, will be coplanar with the incident and deflected guided optical beams. In the case of a three-dimensional coupling, for example, free space to waveguide, the Bragg plane of the grating may be slanted to increase the coupling efficiency. To form a slanted grating coupler which converts a vertical incident wave to a total internal reflection mode with bouncing angle ξ, the two incident angles of the recording beam are

$$\theta_1 = \sin^{-1}(n/n_r(\sin\Delta)) \tag{10}$$

$$\theta_2 = \sin^{-1}(n/n_r(\sin(\Phi-\Delta))) \tag{11}$$

where n is the index of refraction of the hologram and n_r is the refractive index of the medium on top of the dichromated

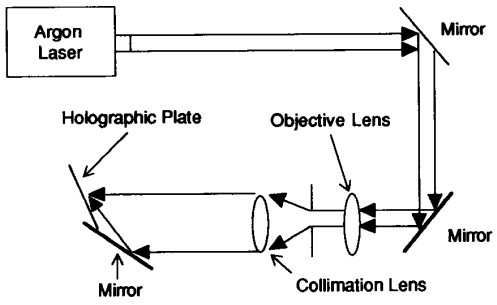

Fig. 3. Recording setup for a waveguide transmission hologram.

gelatin (DCG) hologram ($n_r = 1$ for air) and

$$\Delta = \frac{\Phi}{2} - \sin^{-1}\left(\frac{\lambda_b}{\lambda_r}\left(\sin\frac{\Phi}{2}\right)\right). \tag{12}$$

In Eq. (12), λ_b and λ_r represent the wavelengths of the recording and the reconstruction waves, respectively.

To increase the bouncing distance of the substrate-guided mode, we can either decrease the ratio of λ_b/λ_r by changing the recording and reconstructing wavelengths or increase n_r by putting a high index prism right in front of the holographic plate. To provide high-efficiency diffraction for $\parallel$ or $\perp$ polarized beams, the index modulation Δn associated with the grating shall be

$$\Delta n = \lambda \cos\delta / 2d\varphi \tag{13}$$

where φ is a polarization constant [4] and δ is the Bragg diffraction angle. If all gratings in the one-to-many interconnection architecture have similar Δn values, the maximum number of gratings N that can be fabricated in the same holographic emulsion is estimated to be

$$N = \Delta n_{\max} 2d\varphi / \lambda \cos\delta. \tag{14}$$

In (14), $\Delta n_{\max}$ is the maximum achievable index modulation of the waveguide hologram. For a fixed reconstruction wavelength, we can either adjust the Bragg diffraction angle θ or increase the interaction length d to increase the number of fan-outs. To introduce the desired index modulation, the exposure time t_i for the ith hologram shall satisfy the following equation [3]:

$$t_i = \frac{1}{E\beta}\ell n\left[-\Delta n_i + \left(\Delta n_{\max} - \sum_{j=1}^{i-1}\Delta n_j\right)\right] \div \left[\Delta n_{\max} - \sum_{j=1}^{i-1}\Delta n_j\right] \tag{15}$$

where β is a film sensitivity constant correlated with the holographic material and can be experimentally determined, E is the exposure intensity of the laser beam, Δn_j is the index modulation for the jth exposure, and $\Delta n_{\max}$ is the maximum index modulation for the holographic material. Our calculation shows that the diffraction efficiency is angular dependent and, therefore, to generate equal diffraction efficiency for one-to-many fan-outs, the Δn for each hologram needs to be independently determined. In our angular selectivity calculations, the index modulation for each individual waveguide hologram was fixed at 0.002. The nonlinear response of DPG in (15) is derived from a first-order differential equation representing the film characteristic.

IV. Experimental Results

A. Passive Interconnects

Intraplane guided wave massive fan-out has been demonstrated with 1-to-50 interconnections. Multiplexing all the fan-out holograms is carried out by introducing the optical waves, i.e., objective and reference beams associated with each hologram, to the DCG waveguide emulsion area. The diffraction efficiency of each fan-out beam depends not only on the interaction length but also the optically induced refractive index modulation. The interaction length is defined by the emulsion thickness and the bouncing angle of the guided wave. Index modulation is controlled by the concentration of the photosensitizer and the processing conditions, such as fixing time, exposure dosage, swelling time and dehydration speed. An optimal processing condition provides us with a high percentage of crosslinks as well as full elimination of the active crosslink sites. An alternative recording method to construct the massive fan-out interconnection is to employ multiple exposure beams simultaneously. With m input beams, the total number of gratings thus constructed are

$$N = \frac{m(m-1)}{2}. \tag{16}$$

If $m = 11$, 55 gratings can be made by only one recording. The continuous spectrum of the guided mode defined herein eases the required phase-matching condition. However, the experimental results indicate that the recorded multiplexed holograms are a combination of Bragg and Raman Nath diffractions. Fig. 4 shows the 1-to-many fan-out using six exposure beams simultaneously. Both Bragg and Raman Nath diffractions are observed. Due to the correlation of any two beams, the efficiency and direction of the fan-out beams can not be fully controlled. The 1-to-50 massive fan-out was constructed by recording each individual Bragg grating consecutively through a two-beam exposure method. The result, shown in Fig. 5(a), demonstrates 50 fan-out beams at 514 nm from 30° to 79° with 1° channel separation. The parallel arcs shown here are the scattering caused by the waveguide surfaces. Fig. 5(b) and (c) illustrate the measured diffraction efficiency of 50 beams and the waveguide modes coupled out by a prism coupler. The overall efficiency obtained by summing up all fan-out channels is 55%. Note that diffraction efficiency on 1-to-30 fan-out, as high as 70% at 632.8 nm and 87% at 488 nm, was previously reported [4], [25]. The relatively low diffraction efficiency is believed to be caused by the under dosage of the exposure process.

By integrating a fiber array at the end face of the waveguide or the output prisms surface, board-to-board and wafer-to-wafer interconnects can be realized. A direct 3-D interconnect using a hologram through free space is not practical because of wavelength dispersion. To cover the full spectrum of the

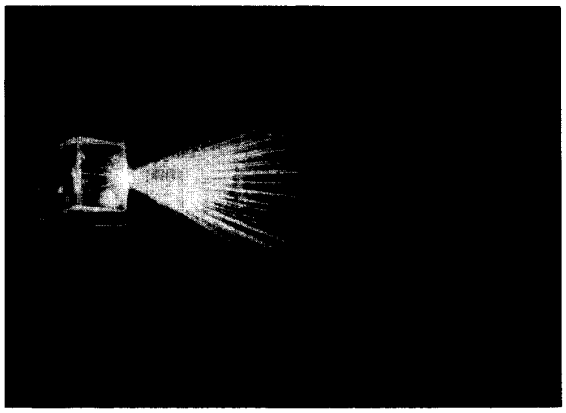

Fig. 4. 1-to-many fan-out at $\lambda = 632.8$ nm using six exposure beams simultaneously. Both Bragg and Raman Nath diffractions are observed.

wavelength of interest, the linear dimension of the detector needs to be enlarged by

$$\ell\Delta\phi = \ell \cdot \left(\frac{\cos\delta'}{\lambda\cos\phi}\right) \cdot \Delta\lambda \tag{17}$$

where ℓ is the distance from the total internal reflection (TIR) hologram to a detector of another optical data bus board, n is the index of refraction of the glass, ϕ is the vertical 3-D board-to-board coupling angle, and δ' is the TIR grating tilt angle. With $\lambda = 632.8$ nm, $\Lambda = 547$ nm, $\phi = 0°$, $\ell = 1$ cm, $\delta' = 23°$, and $\Delta\lambda = 10$ nm. We have $\ell\Delta\phi \approx 17$ μm which will seriously jeopardize the detection bandwidth due to the increase of the detector capacitance ((7)). Implementation of the proposed fan-out architecture, in conjunction with a fiber array embedded in the backplane, is obviously an attractive alternative for providing high speed, highly parallel 3-D optical interconnections. By coupling the guided wave signal from a multiple mode waveguide to a 100/140 multimode fiber through the end face of a prism coupler, 65% coupling efficiency was achieved with an output prism coupler. Note that much higher coupling efficiency is achieved when a microprism coupler ($\sim$100 μm in size) is employed [29]. M-dot has a better match with the guided modes of the fiber. Be aware of the fact that the mode profile of the multimode waveguide demonstrates perfect azimuthal symmetry as do the guided modes of the fiber. As a consequence, optimization of the spot size, i.e., $\sim$100 μm in this case, will provide us with a much stronger overlap integral associated with the coupling efficiency calculation which is

$$C_{\text{eff}} = \sum_{i=1}^{n} \frac{|\langle\Psi_w|\Psi_{f_i}\rangle|^2}{\langle\Psi_w|\Psi_w\rangle \cdot \langle\Psi_{f_i}|\Psi_{f_i}\rangle} \tag{18}$$

when an antireflection coating is applied. In (18), Ψ_w and Ψ_{f_i} represent the mode profiles of the waveguide and the ith mode of the multimode fiber, respectively. Summation over the different modes of the overlap integral are assumed. Employment of a microprism [29] optimizes the mode size of Ψ_w and, thus, maximizes the coupling efficiency C_{eff}. Near-field mode profiles of a 100 μm core size fiber and a multimode waveguide are shown in Fig. 6. Azimuthal symmetry is clearly shown in both cases. The success of coupling from waveguide to fiber (100 μm) was also demonstrated. A 43% coupling efficiency was experimentally confirmed.

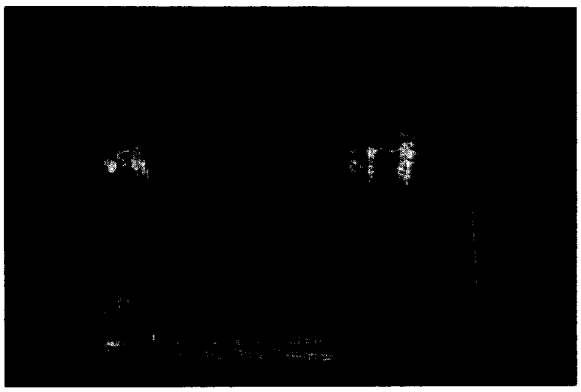

(a)

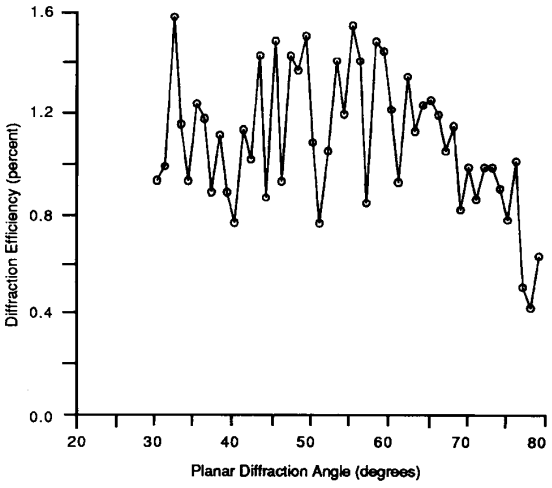

(b)

(c)

Fig. 5. (a) 1-to-50 intraplane guided wave massive fan-out at $\lambda = 514$ nm. (b) Diffraction efficiency of the massive fan-out beams. (c) Mode-dots coupled out from the fanout directions.

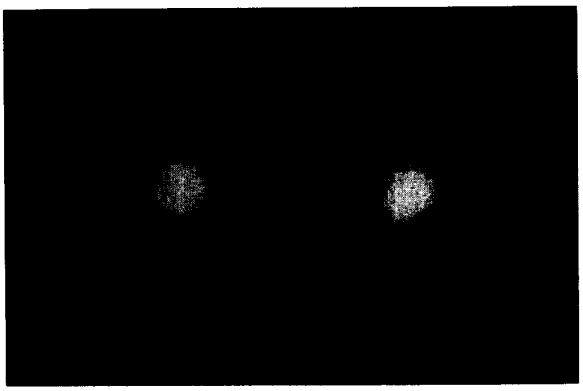

(a) (b)

Fig. 6. Near-field mode profiles of (a) a 100-μm core fiber and (b) a multimode waveguide. Azimuthal symmetry is observed on both cases.

B. Reconfigurable Interconnects

Passive interconnects reported herein represent one of the first demonstrations using optical means to provide massive fan-out intraplane interconnection, which is suitable for routing both data and clock signals. The signals can be modulated by either a laser diode or an external modulator. The on-board reconfigurability is fulfilled by using a Bragg cell. The reconfigurability provides higher parallelity and connectivity and, thus, the number of nodes for the interconnection network. Fig. 7 shows the experimental setup and the experimental results of an acoustically manipulated ON/OFF switching. The Bragg cell was centered at 80 MHz. Note that the data and clock signals can also be provided by using the Bragg cell. The present demonstration is limited by the 3-dB bandwidth of the Bragg cell. The AO modulated signal is routed in the broadcasting mode. 1-to-1, 1-to-many, many-to-1, and many-to-many reconfigurable optical interconnections can be realized by fabricating an appropriately multiplexed hologram array, unlike the single-mode integrated optical device within which multiple signals can only be coplanarly distributed. This multimode structure allows us to transmit modulated signals both collinearly and coplanarly. The collinear distribution of multiple signals is carried out by using different collinear guided modes with distinct bouncing angles and, thus, can be picked up by a discrete on-plane detector. More flexibility is provided. As previously reported [30], on-board switching can be realized by implementing an electrooptic switch, such as a $LiNbO_3$ EO grating to perform similar tasks reported herein. A cascaded switching array can be put into effect while maintaining the compactness of the interconnection network.

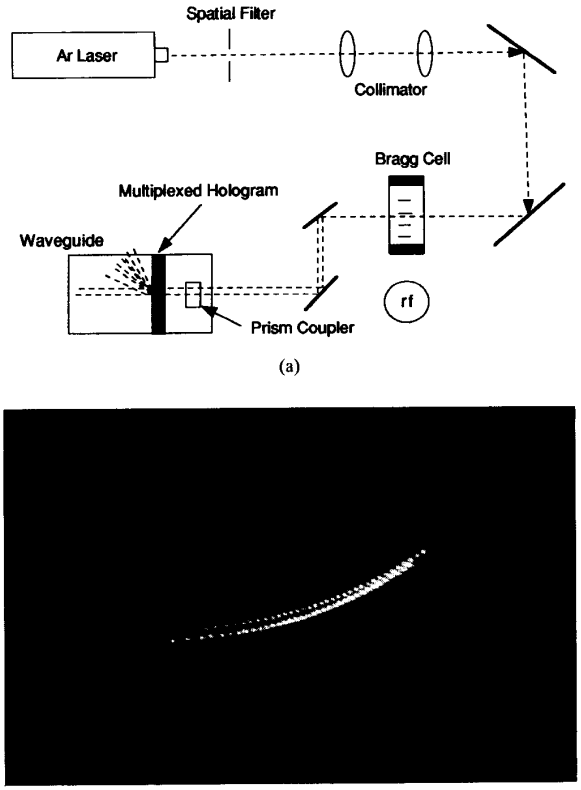

Fig. 7. (a) The experimental setup demonstrating reconfigurable interconnects, and (b) the experimental results of the demonstration. 50 spots (not all shown) can be turned on and off through the AO Bragg diffraction.

V. Reliability Test

A paramount issue that needs to be addressed is the survivability of the multimode waveguide in conjunction with the multiplexed DCG (dichromated gelatin) hologram. It is known that the DCG polymer graft (DPG) is sensitive to environmental humidity. Exposure of the hologram to such an environment degrades the diffraction efficiency significantly. Appropriate protection, such as lamination, hermetic sealing, etc., is needed before this evaluation can be performed [31].

The diffraction efficiency, the diffraction angle, the transmission characteristic, the optical density (OD), and the center wavelength of each transmission grating are tested before and after each temperature cycle. The diffraction efficiency and diffraction angle are measured using an HeNe laser of 632.8-nm wavelength. Excellent stability in optical density, transmission bandwidth, diffraction efficiency, and diffraction angle were found.

A shift in OD peak wavelength was routinely found within the region of -21 ± 3 nm after baking at 180°C for two hours. In the low temperature tests, our experiments were conducted at -66 and -100°C. There were no observable changes after a one hour treatment at both temperatures. The protected sample was also immersed in water for 48 hours and no damage was observed. The spectral response of the sample was examined using a spectrophotometer. A baking test followed immediately afterwards. We have previously reported [31] that the photo-lime polymer withstands 63 MeV protons, up to a total dose of 2 Mrad (Si), and withstands ^{60}Co gamma rays, up to a total dose of 2 Mrad (Si), without loss of diffraction efficiency. Since radiation at such dosages might be expected to disrupt the chemical structure of a polymer, this result suggests that the holographic information might be stored

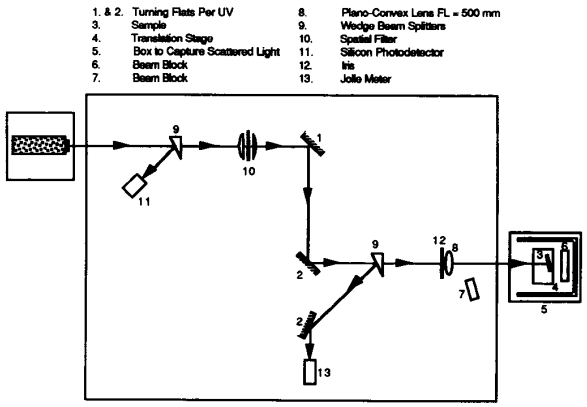

Fig. 8. Schematic of the laser damage threshold tests conducted using a Nd:YAG laser.

in the emulsion through the distribution of physical cracks and fissures formed during the rapid drying step in the post-exposure process. Susceptibility of conventional electrooptic devices to electromagnetic interference (EMI) is primarily due to the involvement of metallic wires and/or thin films. The reported device is based on a multimode glass waveguide and a highly multiplexed DPG hologram and, thus, EMI-immunity is expected.

We have also demonstrated that the DCG hologram we used is extremely stable when exposed to laser radiation. A laser damage test was performed with a Molection Nd:YAG laser that was frequency tripled to operate at 0.3546 μm. Pulse length varied from 8 to 14 ns FWHM. Fig. 8 illustrates the standard laser damage threshold test system. The output of the laser was redirected by several mirrors and passed through an iris that was used to determine the input diameter and to provide a scattered signal to a vacuum photodetector (Hamamatsu R1193U-03), which was used to measure the temporal profile of each pulse.

Pulse intensity was adjusted by a half-wave plate polarizer pair. The beam was filtered and collimated by a spatial filter as well as an iris, and then focused by a $f = 105$ cm planoconvex lens to obtain sufficient exposure of the test sample. The linear dimensions of the Airy disk can be calculated from $d = 1.22\,\lambda f\#$. In our case, $\lambda = 0.3547$ μm, $f\# = 105/.5 = 210$, and $d = 83$ μm. The depth of focus for the lens was large (5 cm) and, as a result, there was a high degree of confidence in having the test plate at the focus.

The test procedure involved marking the areas to be exposed by circling those areas with a 9/16" outside diameter circle and then photographing the marked areas with an American Optical EPT Star Microscope. The area to be exposed on the plate was determined by irradiating the treated area at low intensities. Then the test areas were exposed to pulses of increasing fluency until damage occurred. After each pulse, the irradiated area was examined for damage with a 10× inspection microscope. Following exposure, the damaged areas were again photographed under various magnifications in order to document and identify the extent of damage. A 10 kJ/cm^2 exposure dosage was administered and there was no damage observed. The results of the reliability test are summarized in Table II.

TABLE II
RELIABILITY TEST OF THE WAVEGUIDE DEVICES AFTER LAMINATION

Temperature Stability (−100°C, +180°C), Preserving O.D. > 4.0.
High Laser Damage Threshold (>10 J/cm^2), Following TRW's Standard Nd:YAG Laser Third-Harmonic Test.
Nuclear Radiation-Hardened (Under 63-MeV, Protons > 2 Mrad(Si) and ^{60}Co Gamma Rays > 2 Mrad(Si)), without Loss of Diffraction Efficiency.

VI. FURTHER APPLICATIONS

In contrast to single-mode integrated optic devices, where a high refractive-index film needs to be fabricated, the substrate guided wave massive fan-out optical interconnection reported in this program requires only a transparent substrate at the wavelength of interest. Involvement of the substrate as the guiding medium allows us to route optical signals collinearly and coplanarly. This has one more degree of freedom than that of the single-mode devices. One of the major bottlenecks of implementing integrated optical circuitry on various substrates is the difficulty of fabricating a high index layer with good optical transmission. Our work relaxes that requirement. A two-dimensional data array [32], [33] can be processed using a substrate guided mode. The increased parallelism allows us to fully utilize the advantage of optics in an integrated optics version.

There are a wide array of applications to which this technology seems ideally suited. Backplane optical interconnection, optical clock distribution, surface enhanced Raman Scattering (SERS) sensor, head-up display, intra-plane optical interconnection, and local area networks, appear to be the most promising ones. Integration of an optical backplane with a multiplexed hologram allows us to use the backplane itself as the optical data bus to perform board-to-board optical interconnections. The transmission and receiving of the optical signals from board to backplane to board can be realized using TIR holograms [30]. The optical data bus can be spatially multiplexed without jeopardizing the signal transmission. The use of our interconnection concept on intrawafer interconnections is obvious by employing the substrate as the guiding medium. Unlike the electrical and single-mode waveguide interconnections, the optical data bus described herein does not employ any real estate of the wafer, which has already been intensively occupied by electronic devices, such as memory, logical gates, etc. As a result, high packaging density associated with VLSI and ULSI can be maintained while upgrading the processing speed beyond the limitation of an electrical interconnection. An optical clock distribution using a wafer substrate as the optical clock data bus can also be realized. Fig. 9 illustrates the schematic of a concept which eliminates the clock skews due to the propagation delay. Implementation of a surface emitting laser (SEL) on the same wafer provides us a package with excellent compactness and ruggedness. The SERS sensor has

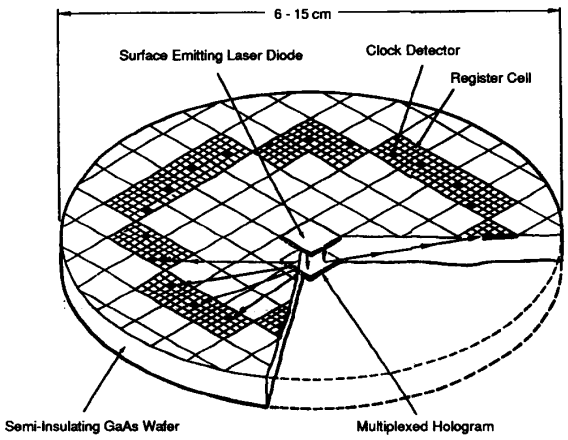

Fig. 9. Optical clock signal distribution for wafer scale integrated circuit.

been intensively investigated due to its excellent sensitivity when compared with a conventional Raman sensor [34]. Implementation of metal-coated moth eye structures [35] on the waveguide surface described in this paper greatly enhance the collection of Raman shifted lines. Finally, the head-up display can be realized using waveguide illumination [36], which maintains the compactness of the system. The pattern to be illustrated can be defined through a hologram or an active absorption plate. Note that the stop light located at the rear window of an automobile can also be made by the reported concept. Using the glass window as the waveguide, in conjunction with a vertical reflection hologram centered at the red wavelength, a stop light located at the rear window with excellent see-through capability can be fabricated.

VII. Conclusions

An increase in the system size and the modulation speed require an alternative interconnection method which eliminates the bottlenecks of current electrical interconnections. In this work effort, we have shown how intraplane guided-wave massive fan-out optical interconnects could be used in conjunction with high efficiency multiplexed HOE's. Our reported methods can be implemented to perform chip-to-chip, intrawafer and board-to-board (through backplane) interconnections. A theoretical calculation is provided to evaluate the angular selectivity, the fan-out density and the power budget. Transformation of the coordinate system has simplified the 3-D diffraction theory into a 2-D problem. $\eta_{\|}$ and $\eta_{\perp}$ can be analyzed independently using the 2-D scheme. The out-of-plane behavior of $\eta_{\|}$ and $\eta_{\perp}$ results in a combined diffraction efficiency of less than 100%. 100% diffraction efficiency can only exist when d and Δn are optimized and the incident beam has a polarization of either $\|$ and $\perp$ polarization. The reported interconnection scheme provides us with not only a coplanar fan-out as the conventional integrated optic device, but also multiple collinear signal routing capability. As a result, the total number of fan-outs can be highly multipled through substrate guided mode interconnection. Recording setup for both an intraplane transmission waveguide hologram and a TIR hologram has been addressed. The required phase matching condition for each hologram is managed by precisely introducing the objective and reference beams simultaneously. Both multiple-mirror (>2) and two-mirror exposure methods were used to provide 1-to-many intraplane guided wave fan-out. The existence of a Raman-Nath diffraction associated with a multiple-beam recording method restricted its usefulness in 1-to-many fan-outs, where each individual output beam has a well-defined direction. Experimental results on a 1-to-50 intraplane guided wave fan-out was conducted at $\lambda = 514$ nm. A combined diffraction efficiency of 55% was observed. Azimuthal symmetry of the guided mode profile allows us to efficiently couple an optical wave into a multi-mode fiber. A reconfigurable optical interconnects were further demonstrated by fabricating an acoustical-optically modulated light beam. 1-to-2-to-100 has been demonstrated with a Bragg cell centered at 80 MHz.

The reliability test of a protected waveguide device in harsh environment was thoroughly evaluated. The results concluded that the laminated DPG-based glass waveguide device is highly reliable in high temperature (to 180°C), low temperature (−100°C), laser radiation (10 kJ/cm^2), high moisture (immersion in water for 48 hours), and nuclear radiation (63 MeV protons to 2 Mrad(ST) and ^{60}Co gamma ray to 2 Mrad(ST)) conditions. Technology applications include backplane optical interconnects, intrawafer clock signal distribution, surface enhanced Raman sensor, and head-up display, etc. The implementation of an interconnection network is solely dependent on the transparency of the substrate. No high refractive-index waveguide, such as GaAs/GaAlAs, Ti:$LiNbO_3$, etc., is needed. Therefore, the reported multi-mode waveguide interconnects can be transferred to any substrate with the require transmission bandwidth.

Acknowledgment

The authors thank Drs. J. Neff, A. Yang, and G. Simonis for their encouragement and continuous support.

References

[1] M. R. Feldman, S. C. Esener, C. C. Guest, and S. H. Lee, "Comparison between optical and electrical interconnects based on power and speed considerations," *Appl. Opt.*, vol. 27, pp. 1742–1751, 1988.
[2] J. W. Goodman, F. J. Leonberger, S. Y. Kung, and R. A. Athale, "Optical interconnections for VLSI systems," in *Proc. IEEE*, vol. 72, pp. 850–865, 1984.
[3] P. R. Haugen, S. Rychnovsky, A. Husain, and L. D. Hutcheson, "Optical interconnects for high speed computing," *Opt. Eng.*, vol. 25, pp. 1076–1085, 1986.
[4] R. T. Chen, M. R. Wang, and T. Jannson, "Intraplane guided wave massive fanout optical interconnections," *Appl. Phys. Lett.*, vol. 57, pp. 2071–2073, 1990.
[5] H. Kogelnik, "Coupled wave theory for thick hologram gratings," *Bell System Technol.*, vol. 48, pp. 2909–2947, 1969.
[6] P. Phariseau, "On the diffraction of light by progressive supersonic waves," *Proc. Indian Acad. Sci. Sect. A*, vol. 44, pp. 165–170, 1965.
[7] W. R. Klein and B. D. Cook, "Unified approach to ultrasonic light diffraction," *IEEE Trans. Sonics Ultrason.*, vol. SU-14, pp. 123–134, 1967.
[8] R. R. Aggrawal, "Diffraction of light by ultrasonic waves," *Proc. Indian Acad. Sci.*, vol. 31, pp. 417–426, 1950.
[9] G. L. Fillmore and R. F. Tynan, "Sensitometric characteristics of hardened dichromated-gelatin films," *J. Opt. Soc. Amer.*, vol. 61, pp. 199–203, 1971.

[10] J. A. Kong, "Second-order coupled-mode equations for spatially periodic media," *J. Opt. Soc. Amer.*, vol. 67, pp. 825–829, 1977.
[11] R. Magnusson and T. K. Gaylord, "Analysis of multiwave diffraction by thick gratings," *J. Opt. Soc. Amer.*, vol. 67, pp. 1165–1170, 1977.
[12] M. G. Moharam and T. K. Gaylord, "Rigorous coupled wave analysis of planar-grating diffraction," *J. Opt. Soc. Amer.*, vol. 71, pp. 811–818, 1981.
[13] M. G. Moharam and T. K. Gaylord, "Rigorous coupled wave analysis of grating diffraction–E-mode polarization and losses," *J. Opt. Soc. Amer*, vol. 73, pp. 451–455, 1983.
[14] T. Tamir, H. C. Wang, and A. A. Oliner, "Wave propagation in sinusoidally stratified dielectric media," *IEEE Trans. Microwave Theory Tech.*, vol. MTT-12, pp. 323–335, 1964.
[15] T. Tamir and H. C. Wang, "Scattering of electromagnetic waves by a sinusoidally stratified half-space: I. formal solution and analysis approximations," *Can. J. Phys.*, vol. 44, pp. 2073–2094, 1966.
[16] T. Tamir, "Scattering of electromagnetic waves by a sinusoidally stratified half-space: II. Diffraction aspects at the Rayleigh and Bragg wavelengths," *Can. J. Phys.*, vol. 44, pp. 2461–2494, 1966.
[17] C. B. Burckhardt, "Diffraction of a plane wave at a sinusoidally stratified dielectric grating," *J. Opt. Soc. Amer.*, vol. 56, pp. 1502–1509, 1966.
[18] L. Bergstein and D. Kermisch, "Image storage and reconstruction in volume holography," *Proc. Symp. Modern Opt.*, vol. 17, pp. 655–680, 1967.
[19] R. S. Chu and T. Tamir, "Guided wave theory of light diffraction by acoustic microwaves," *IEEE Trans. Microwave Theory Tech.*, vol. MTT-18, pp. 486–504, 1970.
[20] R. S. Chu and T. Tamir, "Wave propagation and dispersion in space-time periodic media," *IEEE Proc.*, vol. 119, pp. 797–806, 1972.
[21] F. G. Kaspar, "Diffraction by thick periodically stratified gratings with complex dielectric constant," *J. Opt. Soc. Amer.*, vol. 63, pp. 37–45, 1973.
[22] S. T. Peng, T. Tamir, and H. L. Bertoni, "Theory of periodic dielectric wavelengths," *IEEE Trans. Microwave Theory Tech.*, vol. MTT-23, pp. 123–133, 1975.
[23] R. S. Chu and J. A. Kong, "Modal theory of spatially periodic media," *IEEE Microwave Theory Tech.*, vol. MTT-25, pp. 18–24, 1977.
[24] S. L. Chuang and J. A. Kong, "Wave scattering from a periodic dielectric surface for a general angle of incidence," *Radio Sci.*, vol. 17, pp. 545–557, 1982.
[25] M. R. Wang, G. Sonek, R. T. Chen, and T. Jannson, "Large fan-out optical interconnects using thick holographic grating and substrate wave propagation," *Appl. Opt.*, vol. 31, pp. 236–249, 1992.
[26] R. T. Chen, H. Lu, D. Robinson, and T. Jannson, "Highly multiplexed graded index polymer waveguide hologram for near-infrared eight-channel wavelength division demultiplexing," *Appl. Phys. Lett.*, vol. 59, pp. 1144–1146, 1991.
[27] R. T. Chen, "Multiple mode optical switching array for fiber optic networks," Final Report to Wright Patterson AFB, Contract No. F33657-89-2208.
[28] A. Yariv, *Introduction to Optical Electronics, 2nd Ed.* New York: McGraw-Hill, 1980, ch. 10 & 11.
[29] R. T. Chen, "Optical Interconnects: A solution to very high speed integrated circuits and systems," *Proc. of SPIE*, vol. 1374, p. 20, 1990.
[30] R. T. Chen, M. R. Wang, T. Jannson, and R. Baumkick, "Reconfigurable switching network for multi-mode fiber arrays," *Proc. of SPIE*, vol. 1338, pp. 69–81, 1990.
[31] T. Jannson, G. Savant, and Y. Qiao, "Holographic rugate structures for X-ray optics applications," Final Report to DOE, Contract No. FG03-86-ER13600, 1989.
[32] E. S. Maniloff and K. M. Johnson, "Dynamic holographic interconnects using static holograms," *Opt. Eng.*, vol. 29, pp. 225–229, 1990.
[33] P. Yeh, A. Chiou, and J. Hong, "Optical interconnections using photorefractive dynamic holograms," *Appl. Opt.*, vol. 27, p. 2093, 1988.
[34] P. R. Graves, "Enhanced Raman scattering from thin film chromia substrate," *Tenth Internation. Conf. Raman Spectroscopy*, pp. 5-58–5-29 (Eugene, OR) 1986.
[35] Ray T. Chen, "Holographic lithography for microcircuits," Final Report to Wright Patterson AFB, Contract No. F33615-89-C-1093.
[36] M. M. Down and J. Jahns, "Integrated-optical array generator," *Opt. Lett.*, vol. 15, pp. 769–770, 1990.

Ray T. Chen (M'91) received the Ph.D. degree in electrical engineering from the University of California, Irvine, under the direction of Prof. Chen S. Tsai. He received the M.S. and B.S. degrees in physics from the Universtiy of California, San Diego, and National Tsing Hua University, Taiwan, respectively.

He is currently the director of the Electrooptic Engineering Department at the Physical Optics Corporation. He has been the author and the principal investigator of 20 awarded research proposals sponsored by many subdivisions of DOD, NSF, DOE, NASA, and private industries. His research topics involve 2–D and 3–D optical interconnects, integrated optics. electrooptics switches/modulators, GaAs all-optical crossbars, $X^{(2)}$ nonlinear polymers, polymer waveguides and waveguide modulators, GRIN Polymer Waveguide laser optical fiber sensors, switching networks for fiber sensor arrays, image processing, holographic lithography and holographic optical elements. Together with a UCLA research team, he has recently demonstrated a board-to-board optical interconnect with 60 GHz bandwidth.

Dr. Chen has been the chair as well as a committee member for various SPIE and IEEE conferences. He has more than 70 publications in open literature. He is a member of SPIE, PSC, and OSA

Huey T. Lu is a student at the University of La Verne, CA, where he is pursuing the B.S. degree in optical engineering.

He has been a research assistant at Physical Optics Corporation since 1989. He is currently responsible for research of microstructure polymer waveguides, optical interconnections, a multichannel wavelength division demultiplexer in the near infrared, and holographic optical switching element. Prior to joining the Physical Optics Corporation, he workd on semiconductor laser characterization and packaging at Plesscor Optronics, Inc.

Mr. Lu is a member of SPIE.

Daniel Robinson is a research technician with Physical Optics Corporation Integrated Optics Group, where he has been working for the past two years. He participated in the research, fabrication, and testing of massive fanout holograms for reconfigurable optical interconnect networks. Prior to his current employment, he workd at the NASA Ames-Dryden Flight Loads Research Facility at Edwards Air Force Base.

Michael Wang, photograph and biography not available at the time of publication.

Gajendra Savant, photograph and biography not available at the time of publication.

Tomasz Jannson, photograph and biography not available at the time of publication.